IPC

Indonesian Physics Communication

Department of Physics, Universitas Riau, Pekanbaru, Indonesia
p-ISSN 1412-2960 | e-ISSN 2579-521X

Vol. 21 | No. 3
November 2024

Web: https://kfi.ejournal.unri.ac.id
E-mail: kfi@ejournal.unri.ac.id

Preparation and characterization of Cr-TiO_2/α-Fe_2O_3 nanocomposite for methylene blue degradation

Teguh P. Hadilala[1,*], Erwin Amiruddin[1,*], Amir Awaluddin[2], Rahmondia Nanda Setiadi[1]

[1]Department of Physics, Universitas Riau, Pekanbaru 28293, Indonesia
[2]Department of Chemistry, Universitas Riau, Pekanbaru 28293, Indonesia

*Corresponding author: erwin.amiruddin@lecturer.unri.ac.id; teguh.p7850@grad.unri.ac.id

ABSTRACT

In this study, Cr-TiO_2/α-Fe_2O_3 nanocomposite was prepared by the ball milling method, incorporating chromium, titanium dioxide (TiO_2), and iron oxide (α-Fe_2O_3) nanoparticles extracted from Logas-Kuansing natural sand. The structural, magnetic, morphological, and optical properties of these nanocomposites were investigated using X-ray diffraction (XRD), vibrating sample magnetometer (VSM), scanning electron microscopy (SEM), and UV-Vis spectroscopy. XRD revealed that both the pure and chromium-added nanocomposites have a hexagonal structure, with a crystalline size reduction from 17.5 nm to 19.7, 19.5, and 19.4 nm for the pure and chromium-added samples with chromium concentrations of 0, 5, 10, and 15 wt.%, respectively. Magnetic properties were analyzed through hysteresis loops using VSM, revealing coercivity, saturation magnetization, and remanence magnetization in the ranges of 131 – 247 Oe, 0.80 – 0.54 emu/g, and 0.097 – 0.116 emu/g, respectively. SEM analysis confirmed that the particle shape and size are within the nanometer scale. The optical band gap, estimated using the Tauc relation, decreased from 1.93 eV for the pure nanocomposite to 1.74, 1.68, and 1.72 eV for 5, 10, and 15 wt.% chromium-added nanocomposites, respectively. This study suggests that the prepared Cr-TiO_2/α-Fe_2O_3 nanocomposite exhibits promising physical properties as a catalyst for the degradation of methylene blue.

Keywords: Ball milling; Cr-TiO_2/α-Fe_2O_3; Logas natural sand; nanocomposite

Received 06-09-2023 | Revised 15-10-2023 | Accepted 02-11-2024 | Published 30-11-2024

INTRODUCTION

The rapid growth of industries in recent decades has been remarkable. The discharge of several hazardous dyes from various textile industries into wastewater is a major cause of serious environmental problems that affect human health and aquatic ecosystems, due to the toxicity and carcinogenic effects of these substances. The pollutants released by these industries include oils, pharmaceuticals, cosmetics, photochemicals, and textile effluents [1, 2]. The most commonly used dye in the textile industry is methylene blue (MB). MB is a cationic dye widely used in various industries, including textiles, paper, and plastics. MB is known to be toxic, carcinogenic, and mutagenic [3]. Nanocomposites have garnered significant attention for their potential in environmental remediation, particularly for degrading organic pollutants. Recycling nanocomposites enhances water purification, making it more eco-friendly, efficient, and cost-effective [4]. Natural iron sand contains iron oxide compositions, including magnetite (Fe_3O_4), maghemite (γ-Fe_2O_3), and hematite (α-Fe_2O_3) [5].

Among the various types of metal oxides, iron oxides such as α-Fe_2O_3 are considered one of the most important oxides due to their numerous technological applications ranging from catalysts to biomedical applications and environmental remediation [6]. Hematite (α-Fe_2O_3), as the most stable iron oxide with n-type semiconductor properties (for example = 2.1 eV) [7]. Hematite has a low cost and high corrosion resistance, making it an attractive material for various applications, such as catalysts, pigments, and gas sensors [8]. For a compound to show the photocatalytic property, it should be a semiconductor with a sufficient

band gap to degrade dyes. Metal oxides such as TiO_2, are widely used due to their photocatalytic, catalytic activity, water splitting properties, nontoxicity, low-cost, and stability [9]. Coupling hematite with other semiconductor with higher band gap energy can increase the photocatalytic activity. TiO_2 with high band energy gap (3.0 – 3.2 eV) is suitable for coupling with hematite [10]. Previous researchers used nanocomposites and metal oxides for the photocatalytic degradation of dyes, enhancing activity with transition metals Ag and Au [11, 12]. There are several methods for preparing α- Iron oxide derived from natural sand can be prepared using methods such as high energy milling (HEM), top down, and ball milling. Ball milling is the best choice for nanoparticle preparation because it is simple, efficient, and cost-effective [13].

In this study, iron oxide nanoparticles (α-Fe_2O_3) were prepared from natural sand in Logas Village, Logas Tanah Darat District, Kuantan Singingi Regency, Riau Province, with the addition of titanium dioxide (TiO_2) nanoparticles in a weight percentage (wt.%) ratio of 65:35 using a simple, efficient, and cost-effective ball milling method to obtain the magnetic nanocomposite TiO_2/α-Fe_2O_3. Subsequently, chromium (Cr) nanoparticles were added in wt.% to form the Cr-TiO_2/α-Fe_2O_3 nanocomposite. We investigated the structural, magnetic, morphological, and optical properties of the magnetic Cr-TiO_2/α-Fe_2O_3 nanocomposite, which serves as an effective photocatalyst for the degradation of MB.

EXPERIMENTAL PROCEDURE

Raw Material and Chemical

The raw material used for preparing α-Fe_2O_3 nanoparticles is natural sands collected from Logas Village, Kuansing District, Riau Province. The chemical used for the mixture of α-Fe_2O_3 nanoparticles to form a nanocomposite is titanium dioxide with the addition of chromium with a purity of 99.99%.

Preparation of Cr-TiO_2/α-Fe_2O_3

The separation of iron oxide and non-iron oxide particles was carried out using an iron sand separator (ISS) and NdFeB magnet. The ball milling process was conducted in three stages, each lasting 50 hours, with the separation of iron oxide and non-iron oxide particles at each stage. The product from the fourth stage of ball milling (BM 4) was combined with TiO_2 nanoparticles in a 65 : 35 wt.% ratio and divided into five equal parts by mass. The TiO_2/α-Fe_2O_3 nanocomposite was then further divided into five equal parts and doped with Cr nanoparticles at concentrations of 0, 5, 10, and 15 wt.%. Next, ball milling was performed for 20 hours on each sample, resulting in Cr-TiO_2/α-Fe_2O_3 nanocomposites. The structural, magnetic, morphological, and optical properties of the nanocomposites without Cr and with added Cr were analyzed using X-ray diffraction (XRD), vibrating sample magnetometer (VSM), scanning electron microscope (SEM), and UV-Vis spectrometer.

RESULTS AND DISCUSSION

Structural Analysis

The XRD patterns of the nanocomposites (TiO_2/α-Fe_2O_3) without and with chromium added at various compositions are shown in Figure 1.

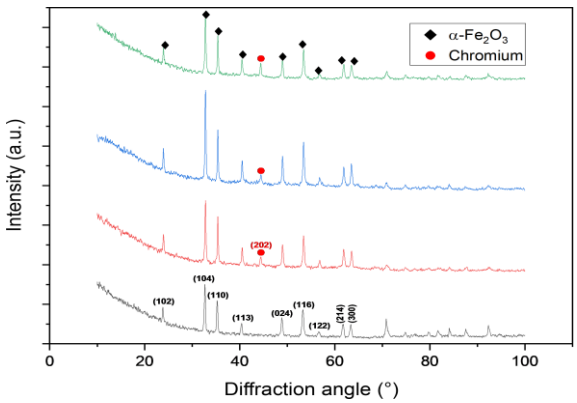

Figure 1. XRD patterns of TiO_2/α-Fe_2O_3 nanocomposites: (a) without chromium and with chromium added at compositions of; (b) 5 wt.%; (c) 10 wt.%; and (d) 15 wt.%.

The patterns were obtained using a Philips X-Ray Diffractometer equipped with Cu Kα radiation with a wavelength of 1.5406 Å. The diffraction patterns of the TiO_2/α-Fe_2O_3 nanocomposites show diffraction peak angles at 23.81°, 32.64°, 35.25°, 40.36°, 48.82°, 53.25°, 56.68°, 61.82°, and 63.36°, which can be indexed to the crystal planes (102), (104), (110), (113), (024), (116), (122), (214), and (300). These peak positions correspond to the standard Bragg positions of hexagonal α-Fe_2O_3, in agreement with JCPDS No. 89-8103.

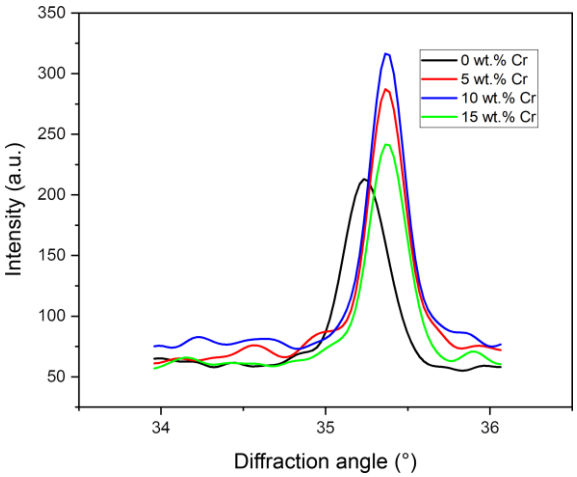

Figure 2. Enlarged diffraction angle from 35.0° to 35.6°, showing a shift of the peak position to a slightly higher angle.

The average crystallite size estimated using the Scherrer formula for the nanocomposites without chromium is 17.5, 19.7, 19.5, and 19.4 nm for chromium compositions of 0, 5, 10, and 15 wt.%, respectively. Additionally, the peak intensity was found to increase, indicating a reduction in crystallite size with the addition of chromium. The XRD pattern also confirmed the presence of an additional diffraction peak at 2θ = 44.37° in the chromium-doped samples. This low-intensity diffraction peak, shown in Figure 1 (b), (c), and (d), indicates the presence of metallic chromium nanoparticles in the samples. Therefore, the presence of diffraction peaks associated with chromium nanoparticles, titanium dioxide, and hematite indicates the success of the ball milling method in forming Cr-TiO_2/α-Fe_2O_3 nanocomposites. As the chromium composition increased, the intensity of the (110) peak was found to increase, as clearly seen in Figure 1. The XRD patterns of the nanocomposites (TiO_2/α-Fe_2O_3) without and with added chromium at different concentrations are shown in Figure 1 and 2.

Magnetic Properties

Figure 3 shows the magnetization (M) curves as a function of the applied magnetic field (H) for the nanocomposites without chromium and with chromium additions (0, 5, 10, and 15 wt.%). The measurements were performed using a VSM in an applied magnetic field ranging from -20 kOe to +20 kOe. The saturation magnetization of the samples was calculated from the magnetization plot against the applied magnetic field. As shown in Figure 3, the magnetization behavior as a function of the applied magnetic field exhibits hysteresis, with the magnetization of the nanocomposites increasing as the applied magnetic field increases and reaching saturation at a high field of 20 kOe. From the Figure 3, it is clear that the samples exhibit ferromagnetic behavior. The saturation magnetization (Ms) and remanent magnetization (Mr) of the sample without chromium (Ms = 0.80 emu/g and Mr = 0.097 emu/g), respectively, decrease with increasing chromium content.

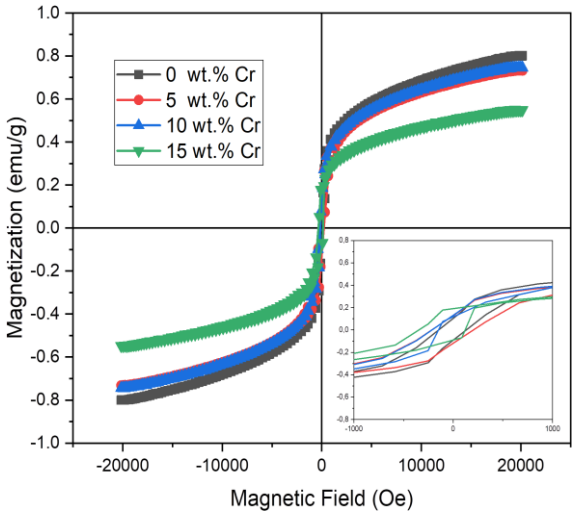

Figure 3. Hysteresis curves of the nanocomposites without and with chromium addition, with an inset showing the enlarged loop of these samples.

The coercivity increases with the addition of chromium, which is attributed to the crystallite size and morphology of the samples, as shown in Figure 4. The increase in the nonmagnetic phase content leads to greater segregation among the nanocomposites, ultimately reducing the magnetization values.

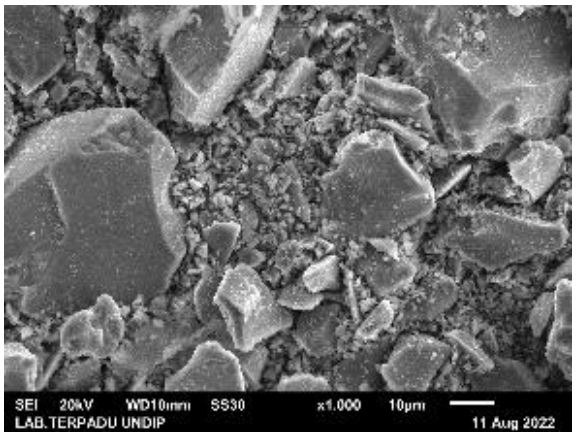

(a)

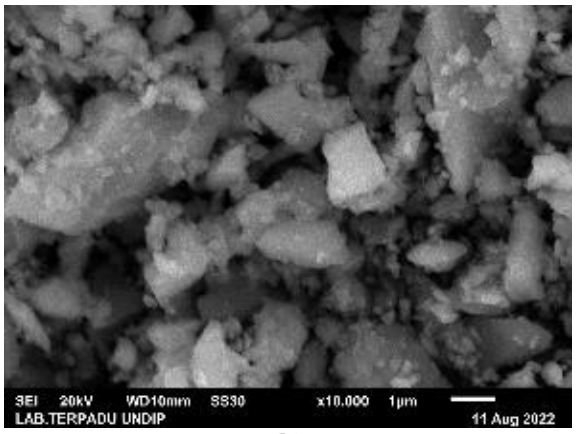

(b)

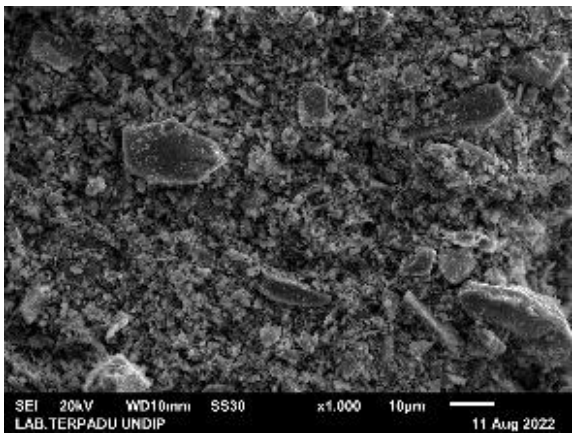

(c)

Figure 4. SEM images of: (a) nanocomposites without Cr; (b) nanocomposites with 10 wt.% Cr; and (c) nanocomposites with 15 wt.% Cr.

Optical Properties

The effect of chromium addition (10 and 15 wt.%) on the optical properties of the nanocomposites was studied based on optical absorption measurements using a UV-Vis spectrometer. The optical absorption spectra of the nanocomposites without chromium and with chromium additions at 5, 10, and 15 wt.% as a function of wavelength, as well as the optical band gap with the average crystallite size and absorption peak as a function of chromium composition, are shown in Figures 5 (a) and 5 (b), respectively.

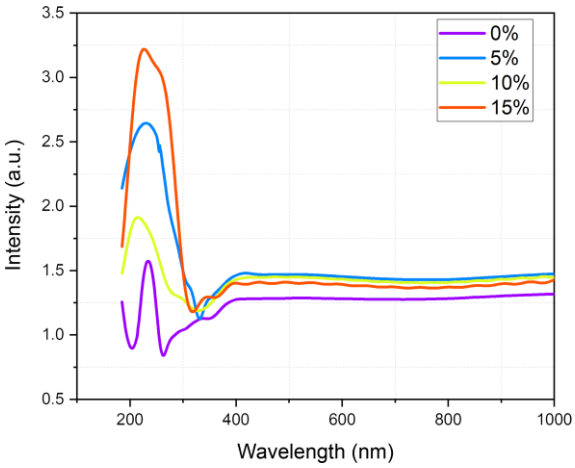

(a)

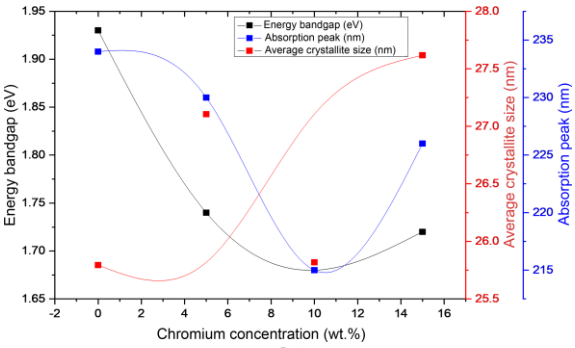

(b)

Figure 5. (a) Absorption spectra of the nanocomposites without chromium and with chromium addition at various compositions; and (b) variation of crystallite size with the optical band gap and absorption peak as a function of chromium composition.

A strong absorption at wavelengths of 234, 230, 215, and 226 nm was observed in the nanocomposites for chromium additions of 0, 5, 10, and 15 wt.%, respectively. This strong

absorption was found to shift towards higher wavelengths, corresponding to lower energy, with increasing chromium concentration, resulting in greater methylene blue degradation.

The optical band gap was obtained by plotting $(\alpha hv)^2$ against photon energy (hv) and extrapolating the linear region (α = 0). The optical band gap was estimated using the Tauc equation:

$$\alpha hv = A\sqrt{E_g - hv} \quad (1)$$

where *h* is Planck's constant, *v* is the frequency, α is the absorption coefficient, and *n* is either 1/2 for direct transitions or 2 for indirect transitions.

The direct band gap of the nanocomposites is shown in Figure 6. The results indicate that the optical band gap calculated through UV-Vis spectroscopy decreased from 1.93 to 1.72 eV as the chromium composition increased from 0 to 15 wt.%. The addition of chromium can narrow the optical band gap of iron oxide nanoparticles. Figure 5 (b) shows the variation of average crystallite size with the optical band gap of the nanocomposites with chromium addition. The band gap of the nanocomposites without chromium and with chromium addition decreased. Therefore, the crystallite size reduced the band gap of the nanoparticles. This is due to the reduction in particle size and average crystallite size, causing the material's band gap to decrease, where the valence band shifts to lower energy and the conduction band shifts to higher energy, resulting in greater methylene blue degradation.

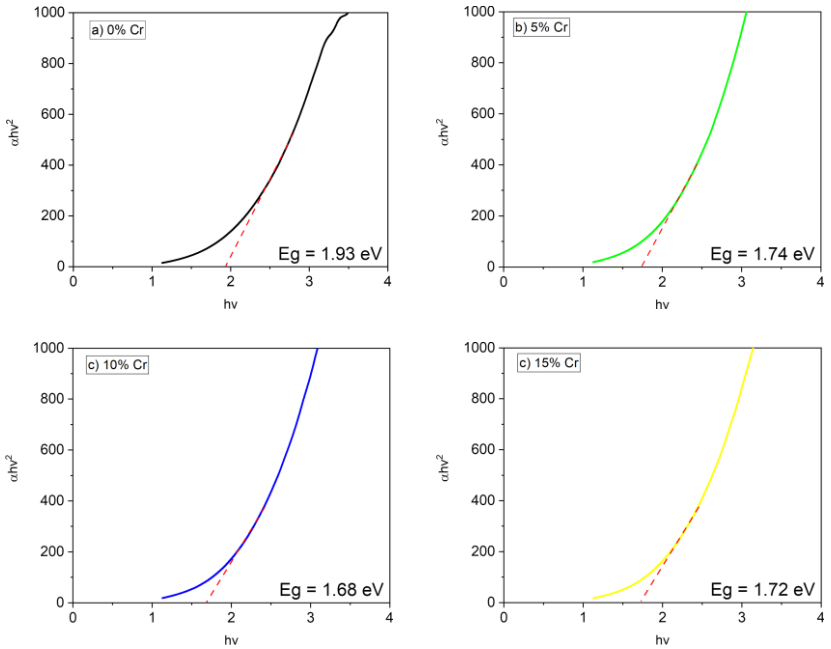

Figure 6. Band gap energy of the nanocomposites without and with chromium addition at various weight percentages.

CONCLUSION

TiO_2/α-Fe_2O_3 nanocomposites with various chromium weight percentages ranging from 0 wt.% to 15 wt.% were successfully synthesized using the ball milling method for methylene blue degradation. Structural characterization studies using XRD revealed that all samples exhibited high crystallinity with a rhombohedral structure. The average crystallite size tended to decrease with increasing chromium content. The success of the ball milling method in forming chromium-added nanocomposites was indicated by the presence of diffraction peaks associated with chromium nanoparticles and TiO_2/α-Fe_2O_3. Magnetic

property studies confirmed the ferromagnetic nature of the samples. The morphological properties showed that nanocomposite agglomeration was more dominant in samples without chromium addition. The optical band gap obtained from Tauc plots showed a decrease with increasing chromium concentration. The results demonstrate that the Cr-TiO_2/α-Fe_2O_3 nanocomposites obtained via this simple ball milling method have the potential as catalysts for methylene blue degradation.

REFERENCES

1. Alwera, S., Talismanov, V. S., Alwera, V., & Domyati, D. (2023). Synthesis and characterization of Sn-doped CeO_2-Fe_2O_3 nanocomposite and application in photocatalytic degradation of Sudan I. *Biointerface Res. Appl. Chem.*, **13**, 179.
2. Ahmed, M. A., El-Katori, E. E., & Gharni, Z. H. (2013). Photocatalytic degradation of methylene blue dye using Fe_2O_3/TiO_2 nanoparticles prepared by sol–gel method. *J. Alloys Compd.*, **553**.
3. Fito, J., Abrham, S., & Angassa, K. (2020). Adsorption of methylene blue from textile industrial wastewater onto activated carbon of *Parthenium hysterophorus*. *Int. J. Environ. Res.*, **14**, 501–511.
4. Tajareh, A. V., Ganjidoust, H., & Ayati, B. (2019). Synthesis of TiO_2/Fe_3O_4/MWCNT magnetic and reusable nanocomposite with high photocatalytic performance in the removal of colored combinations from water. *J. Water Environ. Nanotechnol.*, **4**(3), 198–212.
5. Widodo, R. D., Anis, S., Ichwani, A. A., Setiawan, B., Fitriyana, D. F., & Rochman, L. (2020). Synthesis and characterization of iron (III) oxide from natural iron sand of the south coastal area, Purworejo Central Java. *J. Phys. Conf. Ser.*, **1444**(1), 012043.
6. Erwin, A., Sinuraya, S., Awaluddin, A., Rianna, M., Hadianto, H., Rizki, M., Purba, N. M., & Sitorus, I. T. (2023). Chromium doped iron oxide nanoparticles and physical properties prepared from Logas natural sand and their application in photo-Fenton degradation of methylene blue dye. *ARPN J. Eng. Appl. Sci.*, **18**(10).
7. Ahmad, W. R. W., Mamat, M. H., Zoolfakar, A. S., Khusaimi, Z., & Rusop, M. (2016). A review on hematite α-Fe_2O_3 focusing on nanostructures, synthesis methods and applications. *2016 IEEE Student Conference on Research and Development*, 1–6.
8. Kumar, S., Kumar, M., & Singh, A. (2021). Synthesis and characterization of iron oxide nanoparticles (Fe_2O_3, Fe_3O_4): A brief review. *Contemp. Phys.*, **62**(3).
9. Uzunbayir, B., Kartal, U., Doluel, E. C., Yurddaskal, M., & Erol, M. (2020). Development of α-Fe_2O_3/TiO_2 3D hierarchical nanostructured photocatalysts through electrochemical anodization and sol–gel methods. *J. Sol-Gel Sci. Technol.*, **96**, 441–451.
10. Lubis, S., & Maulana, I. (2018). Synthesis and characterization of TiO_2/α-Fe_2O_3 composite using hematite from iron sand for photodegradation removal of dye. *Jurnal Natural*, **18**(1), 38–43.
11. Mirzaei, A., Janghorban, K., Hashemi, B., Bonavita, A., Bonyani, M., Leonardi, S. G., & Neri, G. (2015). Synthesis, characterization and gas sensing properties of Ag@α-Fe_2O_3 core–shell nanocomposites. *Nanomaterials*, **5**(2).
12. Saber, B. & Mezni, A. (2021). Preparation and characterization of Ag@TiO_2/α-Fe_2O_3 Ternary nanocomposite for enhanced visible light photocatalytic performance. *J. Nanomater.*, **2021**, 12345.
13. Royka, A. & Amiruddin, E. (2021). Penentuan nilai suseptibilitas dan ukuran partikel magnetik pasir alam Logas Kabupaten Kuantan Singingi menggunakan variasi ukuran ball milling. *Komunikasi Fisika Indonesia*, **18**(1).